Materials Science & Engineering A 762 (2019) 138102

Contents lists available at ScienceDirect

Materials Science & Engineering A

journal homepage: www.elsevier.com/locate/msea

Improvement of intrinsic plasticity and strength of $Zr_{55}Cu_{30}Ni_5Al_{10}$ metallic glass by tuning the glass transition temperature

Parijat P. Jana, Abhilash Gunti, Jayanta Das*

Department of Metallurgical and Materials Engineering, Indian Institute of Technology Kharagpur, 721302, India

ARTICLE INFO

Keywords:
Metallic glasses
Glass transition
Strength
Plasticity
Calorimetry
Transmission electron microscopy

ABSTRACT

We report the tuning of the glass transition temperature (T_g) in $Zr_{55}Cu_{30}Ni_5Al_{10}$ metallic glass by rolling at room temperature. The precise thermo-analytical measurements using step-scan modulated temperature differential scanning calorimeter (MTDSC) revealed a decrease of T_g by 16.9 K in ribbons and 7.1 K in bulk glassy plates upon 40% and 70% thickness reduction, respectively. The cold rolled plates exhibit higher yield strength up to σ_y = 1.66 GPa and larger plastic strain (ε_p = 8.0%) before failure than that of as-cast plates (σ_y = 1.45 GPa). Transmission electron microscopy and DSC studies suggest that a relaxed structure has evolved due to the deformation induced structural change upon rolling, which reduces the activation energy of the shear transformation zone and improves the inherent plasticity of the glassy phase.

1. Introduction

Usually, the glass transition temperature (T_g) and the crystallization temperature (T_x) are the two characteristic temperatures, which are used often to characterize any glass-forming liquid [1,2]. The temperature difference between the T_g and T_x is termed as the super-cooled liquid region (ΔT_x), which is the measure of the stability of a glassy phase [3,4]. Hence, T_g is linked with a specific atomic configuration or short-range order (SRO) in the glassy phase, which evolves in the supercooled liquid at a given cooling rate [5]. However, the most stable configuration with lowest free volume content can only be achieved in a metallic glass (MG) solidified at a lower cooling rate, which is rather difficult to achieve precisely during vitrification [6].

The non-equilibrium cooling of the glass forming liquid during vitrification actuates the MGs in a relatively high potential energy state [7]. Now, the MGs can be brought down to a lower potential energy state via a process called structural relaxation. On the other hand, the MGs can be transformed into a metastable state with higher potential energy through a process called structural rejuvenation [7,8]. Both the structural relaxation and rejuvenation can be achieved by the application of thermal treatment and/or stress. The deformation mechanisms and the atomistic processes involved during the relaxation or rejuvenation dynamics of MGs are closely linked with each other [9–11]. The structural relaxation in MGs as a function of temperature starting from the cryogenic temperature up to the glass transition regime and the supercooled liquid region, has been identified as the signature of γ-, β-, α-relaxation, followed by further crystallization [11,12]. However, it is rather difficult to establish the correlation between the potential energy state and a specific structural change. Nevertheless, we can correlate the structural change with the energy storage of the MGs upon plastic deformation, which is confined into the shear bands (SBs) with nano-scale thickness. Recently, it has been established that the structural relaxation or rejuvenation is linked with the fluctuation of the nano-scale properties in the glassy phase [9]. During heating at a moderate rate below T_g, the MGs can achieve a low enthalpy state (i.e., low potential energy) via structural relaxation [13]. The local atomic rearrangement of size ~1–2 nm may occur during the structural relaxation due to the annihilation of the free volume, and the reorganization of the metastable glassy clusters through short- and medium-range ordering of the atoms [14]. However, the sub-T_g (below T_g) annealing can induce embrittlement into the MGs due to the structural relaxation, which can be eradicated by the short time annealing above T_g. Contrarily, the structural relaxation is not the source of the embrittlement during annealing at a temperature above T_g; rather the crystallization is the origin of the embrittlement [15–17].

The plastic deformation of the glassy structure proceeds with the localized atomic rearrangements, which involves stress-induced free volume creation and their annihilation. A steady state flow can be reached when these two processes reach to the equilibrium [18–20]. However, the plasticity of the bulk metallic glasses (BMGs) at room temperature can be improved by either incorporating the ductile phase(s) or the second phase particles with different length scales by choosing the appropriate

* Corresponding author.
E-mail address: j.das@metal.iitkgp.ac.in (J. Das).

https://doi.org/10.1016/j.msea.2019.138102
Received 13 May 2019; Received in revised form 27 June 2019; Accepted 2 July 2019
Available online 04 July 2019
0921-5093/

processing conditions [21,22], or by prior plastic deformation (i.e. cold rolling) [23–30] or surface mechanical treatment (i.e. shot peening) [31]. Along this line, $Zr_{52.5}Ti_5Cu_{18}Ni_{14.5}Al_{10}$ [32], $Zr_{44}Ti_{11}Cu_{9.8}Ni_{10.2}Be_{25}$, $Zr_{55}Ti_5Cu_{20}Ni_{10}Al_{10}$ [21], $Cu_{60}Zr_{20}Ti_{20}$ [33,34], and $Zr_{55}Cu_{30}Ni_5Al_{10}$ [35] BMGs were rolled at room temperature and the improvement of strength, hardness and plasticity have been reported due to the introduction of the microstructural inhomogeneity.

In the present work, we report the tuning of the T_g by cold rolling of $Zr_{55}Cu_{30}Ni_5Al_{10}$ MG with different extent of initial free volume content. Multi-pass cold rolling was employed to examine the effect of rolling on the T_g as measured by the conventional DSC and the step-scan MTDSC. The evolution of the glassy structure in the SBs and the residual glassy matrix, have been examined to interpret the improvement of the strength and plasticity.

2. Experimental

$Zr_{55}Cu_{30}Ni_5Al_{10}$ (*at.*%) ingot was prepared by arc melting of pure Zr, Cu, Ni and Al in Ti-gettered Ar-atmosphere. The detail of the preparation methods of the ribbons and cast plates of $4 \times 2 \times 70\ mm^3$ were reported elsewhere [36]. Both the ribbons and plates were cold rolled (CR) up to 40% and 70% of the initial thickness, respectively, using a rolling apparatus (Carl Wezel KG, Mühlacker, Germany) with 100 mmØ rolls. The ribbon specimens have been collected after achieving engineering strain of 10% (RCR10), 13% (RCR13), 18% (RCR18), 25% (RCR25), 31% (RCR31), and 40% (RCR40), whereas, the plate specimens were collected at a strain of 10% (PCR10), 20% (PCR20), 31% (PCR31), 51% (PCR51), and 70% (PCR70). The samples were dipped into water immediately after each pass, which was kept at ambient temperature (298 K) to avoid the effect of temperature rise upon rolling.

The mechanical properties of the as-cast (PCR0) and CR plates were investigated under compressive load using H50KS TINIUS Olsen universal testing machine at an initial strain rate of 8×10^{-4}/s at room temperature. All the surfaces of the samples were polished using diamond suspension of 3 μm before the test, and the aspect ratio of the parallelepiped samples was kept at 1.9. The deformed samples and the fracture surface of the samples were examined using a field emission scanning electron microscope (FESEM, Zeiss, Merlin, Gemini 2) at an operating voltage of 15 KeV. A high-resolution x-ray diffractometer (XRD, Philips PANalytical PW3373, Netherlands) with Cu–Kα radiation was used for structural investigation. A JEOL JEM 2100F (Japan) high-resolution transmission electron microscope (HRTEM) was used to explore the evolution of structure upon CR. The thermo-analytical measurements were performed using a PerkinElmer DSC8000 differential scanning calorimeter (DSC) under a flow of N_2 gas in the temperature range of 293 K and 783 K. Step-scan MTDSC was performed in the temperature range of 573 K and 753 K with steps of 1 K at 5 K/min with 180 repetitions. Small specimens of ~20 mg were cut from the ribbons and plates for both conventional DSC and step-scan MTDSC experiments. The thermogram of an empty aluminium pan was used to establish the baseline for conventional DSC and step-scan MTDSC measurements.

3. Results

3.1. Compression test

Fig. 1 shows the engineering stress-strain plots showing the brittle behavior of the PCR0 without any hint of macroscopic plasticity. Whereas, the PCR31 displayed large compressive plasticity up to $\varepsilon_p = 8\%$ before failure. The ultimate compressive strength (σ_{max}) increases from 1.45 GPa for PCR0 plate to 1.88 GPa for PCR31. A few more engineering stress-strain curves of differently CR specimens are shown in Fig. 1(a), which shows similar deformation characteristics. The FESEM secondary electron (SE) image of the fracture surface of the

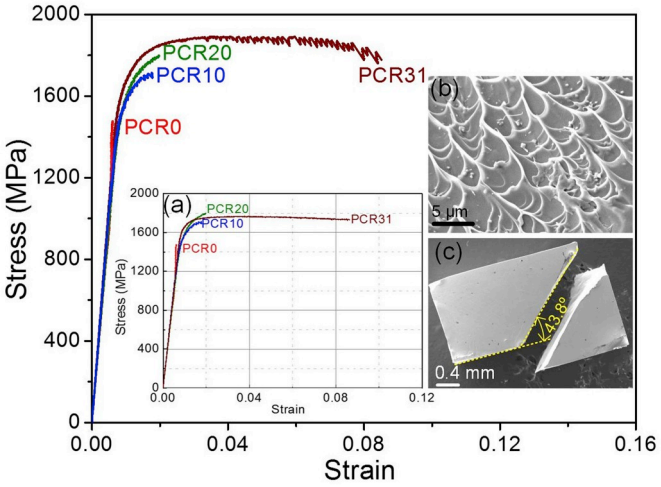

Fig. 1. Engineering stress versus strain curves under compression for as-cast (PCR0) and rolled $Zr_{55}Cu_{30}Ni_5Al_{10}$. Inset (a): the second set of stress-strain plots; Inset (b): the morphology of the fracture surface of PCR0; Inset (c): shear failure at an angle of 43.8° with the compressive loading axis in PCR0.

PCR0 shows the characteristic vein-like pattern, as depicted in Fig. 1(b). The macroscopic view of the PCR0 and PCR31 shows that shear failure has occurred at an angle (θ_f) of 43.8° and 43.6° with the compressive loading axis, respectively, as depicted in Fig. 1(c). The large enhancement of the compressive plasticity and the strength of differently CR specimens are consistent with that reported in the literature for other BMGs [23,37–39].

3.2. Structural and microstructural characterization

The XRD patterns of ribbons and plates subjected to different extent of cold rolling show the characteristic broad diffraction peak pointing the presence of the amorphous phase in the CR and as-spun ribbon (RCR0) as well as PCR0 specimens, as depicted in Fig. 2. No sharp peak of the crystalline phase has been detected in any of the XRD patterns.

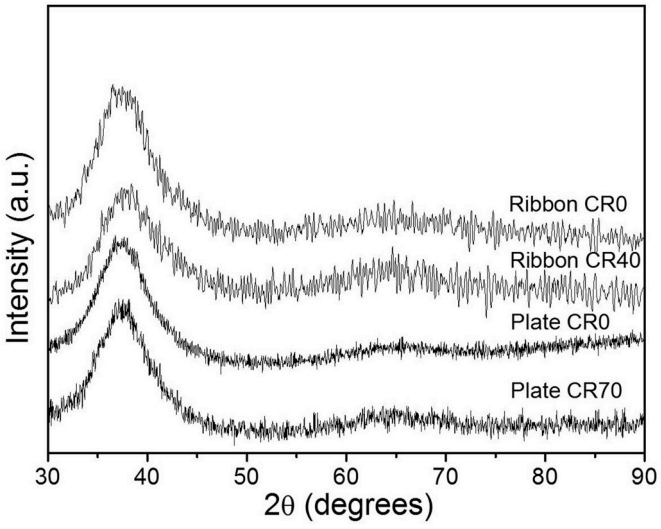

Fig. 2. XRD patterns of the as-spun ribbon (RCR0), 40% CR ribbon (RCR40), as-cast plate (PCR0), and 70% rolled plate (PCR70) of $Zr_{55}Cu_{30}Ni_5Al_{10}$ showing the amorphous nature of the specimens before and after rolling.

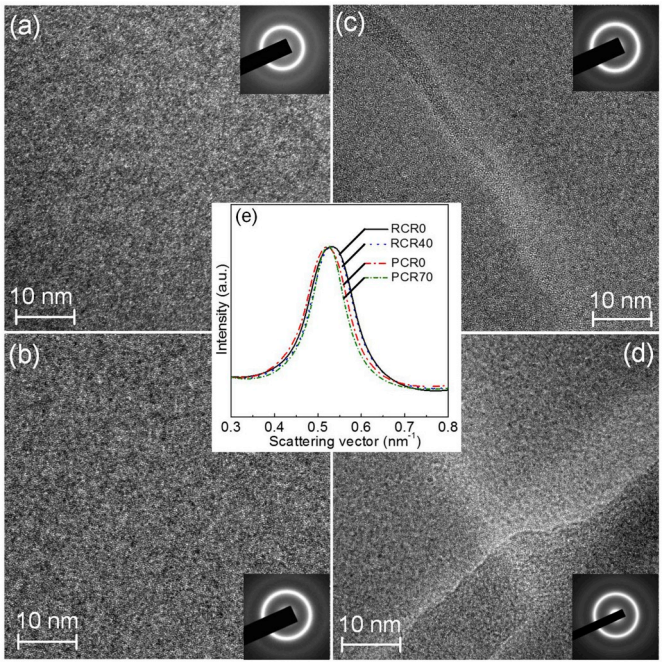

Fig. 3. HRTEM images of the (a) as-spun ribbon (RCR0), (b) as-cast plate (PCR0), (c) 40% rolled ribbon (RCR40), and (d) 70% rolled plate (PCR70). Inset: shows the corresponding SAED patterns. Inset at center: azimuthally integrated intensity profiles of the SAED patterns.

The HRTEM images of the RCR0 and PCR0 exhibit a featureless contrast pointing the glassy nature of the specimens, as shown in Fig. 3(a and b), respectively. The selected area electron diffraction patterns (SAED) of the corresponding images further confirm the diffuse scattering of the glassy structure, as shown in the inset of Fig. 3(a and b). On the other hand, Fig. 3(c and d) show the HRTEM images of RCR40 and PCR70, respectively. The presence of SBs with brighter contrast has been observed along with the featureless glassy matrix, in both the CR ribbons and CR plates. The SAED patterns consist of a diffused halo surrounded by a weaker halo, which are typical for glassy structure, as shown in the inset to Fig. 3(c and d). Hence, the glassy structure remains as glassy after cold rolling of the CR ribbon and CR plate specimens.

In order to study the structure of the glassy phase, SAED patterns have been taken from the glassy phase near to the brighter SBs of the RCR40 and PCR70 plate. These SAED patterns were azimuthally integrated, as shown in Fig. 3(e). The integrated intensity of the SAED patterns from the RCR0 and PCR0 specimens are also shown for comparison. The exposure parameters for capturing all the SAED patterns from different regions of the glassy structure were the same. The structure of the RCR0, PCR0 and the CR specimens are appeared to be similar. The position and the full width at the half maxima (FWHM) of the broad maxima from the different glassy structure are indistinguishable. Furthermore, the Fourier filtered HRTEM images of RCR40 and PCR70 are shown in Fig. 4(a) and (b), respectively. A threshold has been chosen to reveal the features in Fig. 4(a and b) and the contrast of these images have been inverted to represent the bright features using black dots. The presence of these dots confirms that nano-voids have been evolved preferably into the shear bands, as illustrated for RCR40 and PCR70 specimens in Fig. 4(c) and (d), respectively. Actually, the black dots represent the location of voids and not their size. The Fast Fourier transformation (FFT) spectra were taken at the SB, and the nearby matrix in RCR40 and PCR70, which were azimuthally integrated and the ratio of the amplitude is shown as Y-axis in Fig. 5. Prominent peaks near the scattering vector of 0.5 nm^{-1} were observed as marked by arrows in Fig. 5, confirming a structural change at the shear bands [40,41].

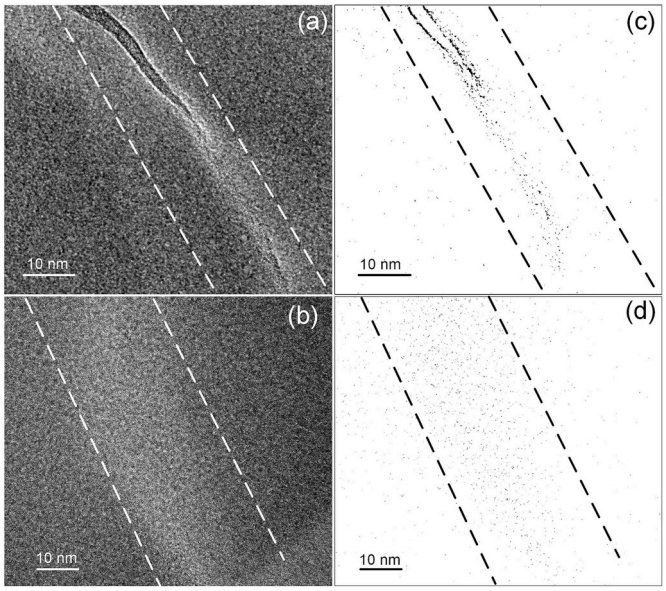

Fig. 4. (a) Fourier filtered image (a) RCR40, (b) PCR70 showing shear bands. (c,d): Contrast inverted image of (a) and (b) after changing the threshold value to represent the formation of nano-voids in the shear band using black dots.

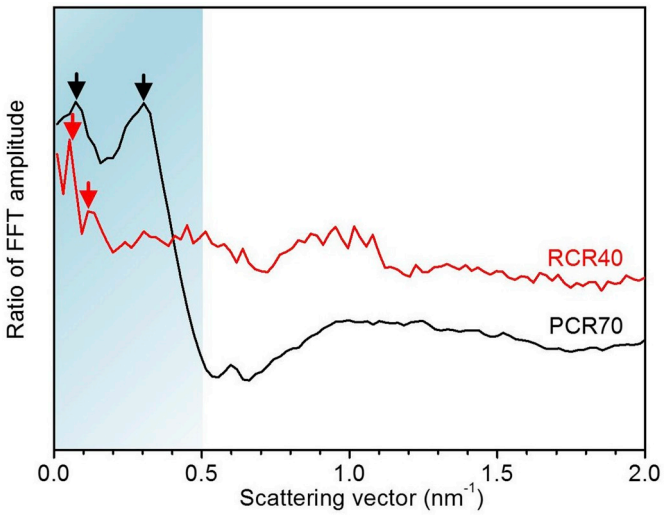

Fig. 5. The variation of the ratio of the FFT amplitude at the shear bands and glassy matrix with scattering vector in 40% rolled ribbon (RCR40) and 70% rolled plate (PCR70). The pronounced peaks are visible below 0.5 nm^{-1} pointing structural modifications in the glassy phase in RCR40 and PCR70.

3.3. Conventional differential scanning calorimetry (DSC)

Fig. 6(a) depicts the conventional DSC curves of the PCR0 and differently CR plates at a heating rate of 20 K/min. All the specimens exhibit an endothermic glass transition event followed by an exothermic crystallization. A magnified view of the DSC trace of PCR0 specimen near T_g is shown to represent the adopted methodology for measuring the characteristic temperatures. These temperatures are the onset of glass transition (T_g^{onset}), the inflection point of the glass transition ($T_g^{inflection}$), and the end of glass transition (T_g^{end}). The $T_g^{inflection}$ is defined as the temperature, where the double derivative of the heat flow versus temperature plot changes from positive to negative when the convention of endothermic event is along the upward direction. Therefore, the T_g^{onset} is defined as the temperature of intersection between the tangent at $T_g^{inflection}$ and the tangent at the left limit of the temperature. Whereas, the T_g^{end} is defined as the intersection

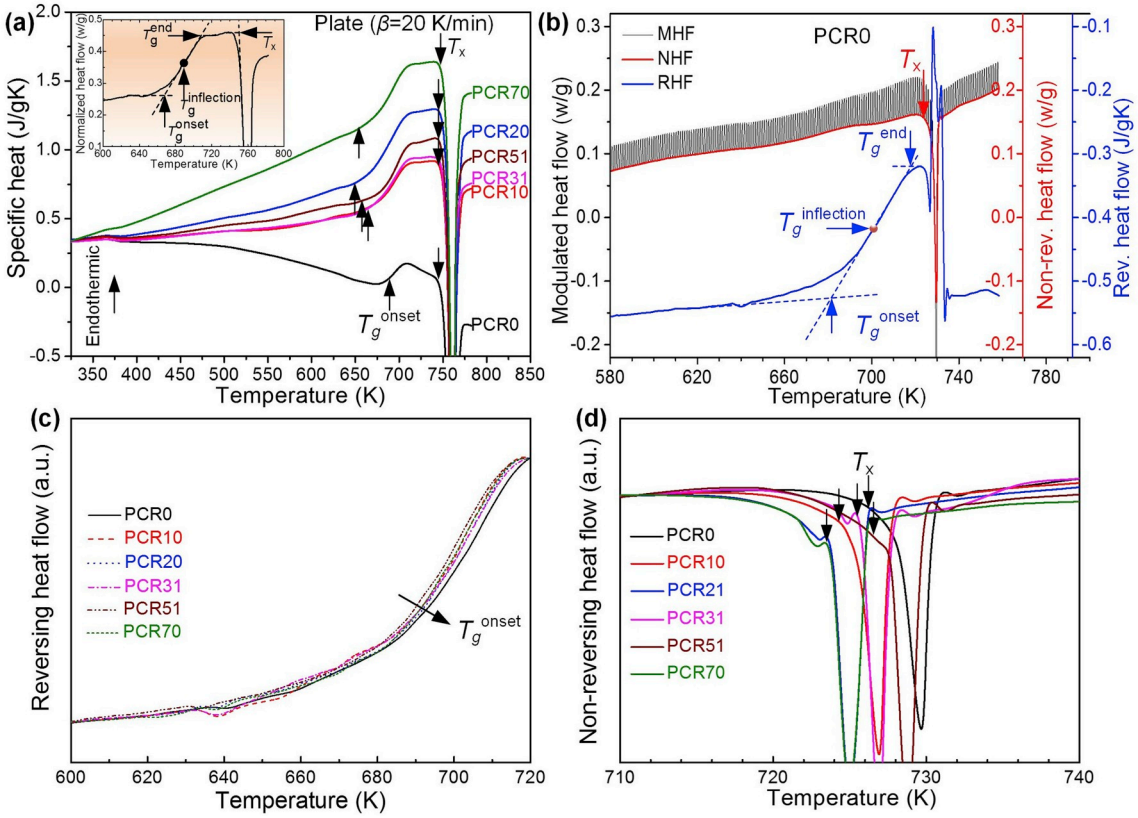

Fig. 6. (a) Conventional DSC curves of PCR0 and differently CR plates at a heating rate of 20 K/min. Inset: DSC thermogram of the PCR0 showing the measurement method of the characteristics temperatures such as, T_g^{onset}, $T_g^{inflection}$, T_g^{end} and T_x. (b) Step-scan MTDSC traces of PCR0 separating the MHF, RHF, and NHF curves. (c) A magnified view of the RHF traces of PCR0 and CR specimens depicting the decrease of T_g^{onset} upon cold rolling. (d) The enlarged view of the NHF traces of the PCR0 and CR plates showing the change of the T_x values upon cold rolling.

temperature of the tangent at $T_g^{inflection}$ and the tangent at the right limit of the temperature. In the present study, we have used T_g^{onset} value to represent the T_g. The onset of crystallization (T_x) is calculated by finding the intersection of the tangent of the left limit of the crystallization peak and the extrapolated tangent at the inflection point of the leading edge of the crystallization peak. The T_g^{onset} and T_x of plate specimens are marked by arrows in Fig. 6(a). The conventional DSC traces of RCR0 and CR ribbons at a heating rate of 20 K/min are shown in Fig. S1(a) [see supplementary]. The RCR0 ribbon exhibits T_g^{onset} of 688.8 ± 4.7 K, which decreases down to 664.0 ± 7.1 K for RCR40 ribbon sample. Whereas, the T_x value for RCR0 ribbon has been estimated to be 760.2 ± 0.6 K and remains almost similar in RCR40 (T_x = 760.3 ± 0.7 K). On the other hand, the T_g^{onset} for PCR0 has been estimated to be 678. 5 ± 3.9 K, which decreases down to 660.2 ± 8.2 K in PCR20 and 674.3 ± 4.3 K in PCR70. However, the T_x values remain almost similar for all the differently CR specimens and lie in the range of 760.0 ± 0.6 K to 762.5 ± 2.5 K. The values of T_g^{onset}, T_x, and ΔT_x are estimated using conventional DSC traces as shown in Table S1 [see supplementary]. Hence, the conventional DSC results suggest that the rolling decreases the T_g^{onset} and modifies the structure as well as the thermal stability of the glassy phase.

3.4. Step-scan MTDSC

Recently, it has been reported that the glass transition temperature can be measured precisely using step-scan MTDSC [36]. Therefore, the effect of rolling on the change of T_g has been further investigated in the present study. The DSC signal arises due to relaxation induced thermodynamic changes in a glassy structure can be easily separated using step-scan MTDSC. The input program in a step-scan MTDSC consists of isothermal segments as well as small heating segments unlike in conventional DSC, where, a heating scan is only used during the entire temperature range of interest. It is well established that the glass transition is always manifested by a change in the specific heat (C_p) at the T_g^{onset}. The deconvolution of the step-scan MTDSC signal provides the non-reversing heat flow (NHF) curve, from which the kinetic information such as relaxation and crystallization events can be obtained. Whereas, the glass transition, and the curing event can be obtained from the reversing heat flow (RHF) curve. Fig. 6(b) exhibits the step-scan MTDSC plots for PCR0, and the same for RCR0 as shown in Fig. S1(b). The deconvolution of the MTDSC heat flow plot produces the modulated heat flow (MHF), RHF, and NHF curves. The RHF represents the thermodynamic information, and the NHF represents the kinetic information of the glassy phase [42,43]. Therefore, the T_g^{onset} and T_x have been determined from the RHF and NHF curves, respectively. Fig. 6(c and d) show the magnified view of the RHF and NHF curves of the PCR0 and differently CR plates, respectively. The RHF and NHF traces of RCR0 and differently CR ribbons are shown in Figs. S1(c and d). The T_g^{onset} of RCR0 has been estimated to be 700.5 ± 0.6 K, which decreases down to 683.6 ± 1.2 K for RCR40 ribbon. Similarly, the T_x value of the RCR0 is 729.2 ± 0.5 K, which decreases down to 726.8 ± 4.2 K for RCR40. Whereas, the T_g^{onset} of PCR0 has been estimated to be 687.0 ± 1.1 K, which has decreased to a lower value of 681.6 ± 2.9 K in PCR70 upon rolling. Moreover, the T_x value for PCR0 is estimated to be 727.8 ± 1.3 K, which has decreased to 724.6 ± 0.9 K for PCR70. The values of T_g^{onset}, T_x and ΔT_x have been estimated using RHF and NHF traces of step-scan MTDSC, as shown in Table S1.

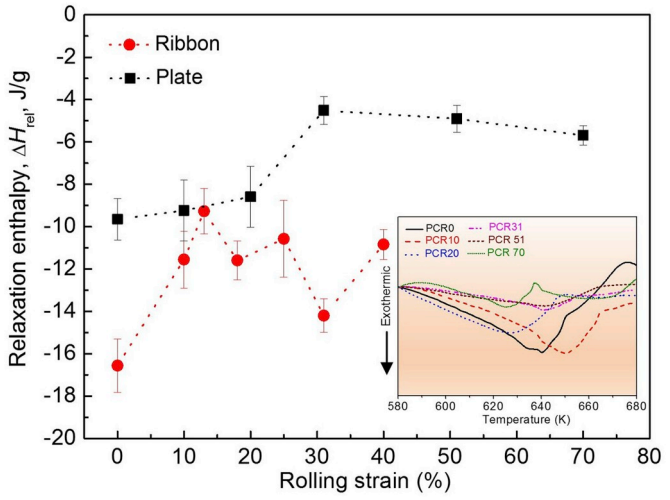

Fig. 7. The variation of relaxation enthalpy (ΔH_{rel}) of MG ribbons and BMG plates rolled to different rolling strain, as estimated from NHF curve of step-scan MTDSC. Error bars in the plot are the standard deviation of the measurements. Inset at right side: The NHF curves for as-cast and CR plates showing the exothermic relaxation peak prior to glass transition.

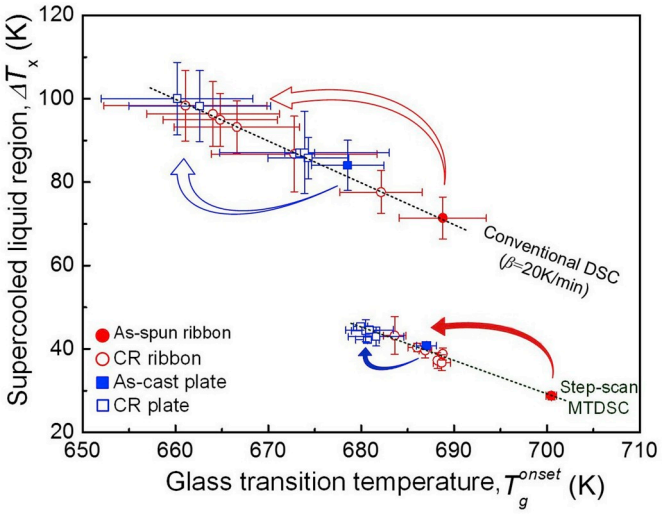

Fig. 8. The T_g^{onset} and ΔT_x values as obtained from both conventional DSC (heating rate: 20 K/min) and step-scan MTDSC for as spun ribbon (filled circle), as-cast plate (filled square) and differently CR ribbons (empty circle), and CR plate (empty square) of $Zr_{55}Cu_{30}Ni_5Al_{10}$. The precise measurements of T_g^{onset} using step-scan MTDSC and the decrease of the T_g^{onset} upon cold rolling are evident. The error bars are the standard deviation values.

4. Discussion

4.1. Effect of cold rolling on relaxation enthalpy and free volume

The relaxation enthalpy (ΔH_{rel}) prior to glass transition of RCR0, PCR0, and differently CR specimens has been estimated from the NHF curves as obtained from the step-scan MTDSC studies. The inset of Fig. 7 shows the NHF curves near to the glass transition for PCR0 and differently CR plates. The exothermic peak in the NHF curve is the indication of the structural relaxation prior to the glass transition. Fig. 7 displays the variation of ΔH_{rel} with the rolling strain for both ribbons and plates. During heating, the exothermic peak prior to the glass transition is indicative of the amount of free volume present in the glassy structure [44]. The exothermic ΔH_{rel} of RCR0 and PCR0 have been estimated to be 16.57 ± 1.26 J/g and 9.65 ± 0.98 J/g, respectively. Whereas, the ΔH_{rel} values of RCR40 and PCR70 have been estimated to be 10.85 ± 0.70 J/g and 5.69 ± 0.46 J/g, respectively. The decrease of ΔH_{rel} upon cold rolling points the reduction of absolute free volume (Δv_f) of the glassy phase. The enthalpy change for the CR samples due to structural relaxation is estimated as the difference of ΔH_{rel} between the as-spun/as-cast and CR samples. The values of the enthalpy change for PCR10 and PCR70 samples are 0.41 J/g and 3.96 J/g, respectively, which corresponds to the reduction of Δv_f by 0.55% and 5.37%, respectively, as estimated according to the correlation described in Ref. [44]. Similarly, the enthalpy change for RCR10 and RCR40 specimens are 5.01 J/g and 5.72 J/g, which is equivalent to the reduction of Δv_f by 6.79% and 7.76%, respectively. The decrease of ΔH_{rel} and the reduction of free volume in CR specimens as compared to the as-spun/as-cast specimens, are the tangible clues pointing that the cold rolling produces a relaxed glassy structure. The relaxation process in the MGs/BMGs reduces the quenched-in internal stresses or quenched-in defects (free volume) [21,45]. The accumulation of the free volume is more in the SBs than the surrounding glassy matrix, which finally appeared as nano-voids, as depicted in Fig. 4(a–d). But apart from the SBs, the free volume in the overall glassy structure reduces. The reduction in free volume near the SBs dominates over the increase in free volume inside SBs. As a result, there is a net decrease of the absolute free volume content in the specimen upon cold rolling. Therefore, the above experimental findings confirm that the structural relaxation is accompanied by the reduction of net free volume content upon cold rolling.

4.2. Effect of cold rolling on the evolution of structure, stability and T_g^{onset}

The DSC and step-scan MTDSC results revealed that the thermal stability of the ribbons and plates has been altered upon cold rolling. Since the characteristic T_g^{onset} and T_x temperatures are linked to a particular configuration of a given glass, therefore, the glassy structure has been configured into a different state of internal energy after each pass of rolling. Hence, the decrease of T_g^{onset} points that the atomic configuration of the glassy phase must have been changed to a thermodynamically more stable state by the work done during rolling. The XRD, HRTEM and FFT studies indicate that the glassy phase remains as glassy in both the ribbon and plate specimens after cold rolling. Fig. 8 shows that the ΔT_x value increases with the decrease of T_g^{onset} in both conventional DSC and step-scan MTDSC. The large value of ΔT_x suggests that the glassy phase possesses more stable configuration after cold rolling.

The mechanism of the inelastic deformation of the glassy phase has been explained using the concept of the shear transformation zones (STZs) theory comprising of the local cluster of atoms and free volume/flow defects. The plastic deformation of the glassy phase confined into these STZs, which sequentially propagate and form microscopic SBs. However, the surface of the glassy ribbons and plates exhibit the propagation and intersection of SBs upon cold rolling, as depicted in Fig. 3(a–d). The rate of activation of STZs ($\dot{s}$) could be favored or opposed by the applied shear stress (τ) as follows [46,47]:

$$\dot{s} = \nu_0 \exp\left(-\frac{Q \pm \tau V}{kT}\right) \quad (1)$$

where, k is the Boltzmann constant ($k = 1.3807 \times 10^{-23}$ J/K), Q is the activation energy of the process, V is the activation volume, and ν_0 is the shear distortion frequency of a STZ. Similarly, the free energy associated with the formation of a STZ is also linked with the Poisson's ratio (ν) as [46]:

$$\Delta F_0 = \left[\frac{7-5\nu}{30(1-\nu)} + \frac{2(1+\nu)}{9(1-\nu)}\beta^2 + \frac{1}{2\gamma_0}\cdot\frac{\tau_0}{\mu(T)}\right].\mu(T).\ \gamma_0^2.\ \Omega_0 \quad (2)$$

where, $\mu(T)$ is the temperature dependent shear modulus, and τ_0 is the required shear stress to activate STZ. Ω_0 and γ_0 are the characteristics STZ volume and strain, respectively. β is the ratio of the dilatation to shear strain. The activation of a STZ will be favored when the value of Q

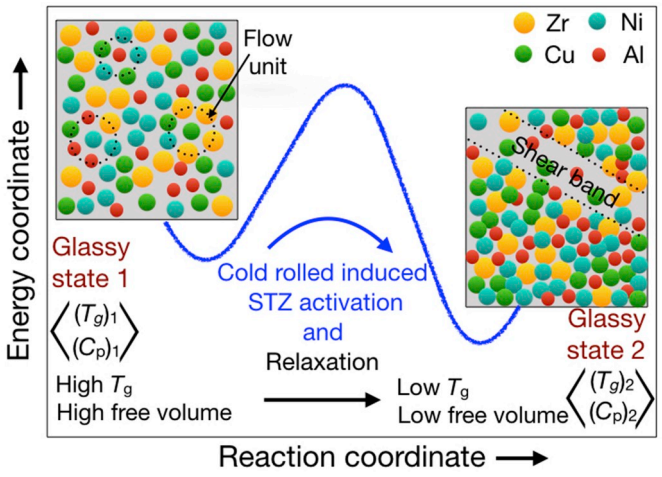

Fig. 9. A schematic representation of the cold rolling induced structural relaxation process in as-spun/as-cast metallic glasses. The black dotted circles represent the flow units. The black dotted lines indicate the shear band, which has evolved upon cold rolling.

of Eq. (1) equals to the value of ΔF_0 in Eq. (2). The value of the ΔF_0 is directly linked with the T_g value as ~20–120 kT_g, as stated in Ref. [46]. In the present case, we have considered the value of $\Delta F_0 = 20kT_g$. Therefore, the decrease of T_g^{onset} upon rolling essentially has lowered the ΔF_0 value of STZs, which further points the evolution of newer configuration in the glassy structure to a more relaxed state than that of as-cast/as-spun glassy specimens. The value of ΔF_0 of STZs is estimated to be 19.34×10^{-20} J and 18.97×10^{-20} J for as-spun ribbon and as-cast plate specimens, respectively, which has decreased to 18.88×10^{-20} J and 18.77×10^{-20} J upon rolling. It should be noted that the activation energy for crystallization in $Zr_{55}Cu_{30}Ni_5Al_{10}$ BMG has been reported to be 57.12×10^{-20} J, which is 3 times higher than that of ΔF_0 of STZs [48]. Hence, the formation of STZs become easier upon rolling, which further increase the macroscopic shear band density, reduce the shear band spacing and increase the compressive plasticity. A schematic illustration of the cold rolling induced relaxation process in metallic glass is shown in Fig. 9 pointing that the atomic configuration with higher energy shows a higher T_g value due to the evolution of higher free volume content in the specimen. Conversely, the low potential energy configuration of the glassy phase is correlated with the lower T_g value and reduced free volume content. The work done during cold rolling provides the activation energy for the configurational change in the glassy phase from state 1 to state 2.

4.3. Effect of cold rolling on strength and plasticity

The intrinsic plasticity and the strength of a glassy phase depend on the net free volume content in the glassy phase, their distribution throughout the specimen as well as the rate of free volume creation and structural relaxation during plastic deformation. Heggen et al. had derived a relation between the rate of free volume (ν_f) creation and the applied stress (σ) for the steady state flow [49]:

$$\frac{d\nu_f}{dt} = a_x \gamma \nu^* \frac{d\varepsilon}{dt}\sigma \tag{3}$$

ν^* is the critical free volume for atomic diffusion, γ is the geometrical overlap factor between 0.5 and 1, $a_x = (\Omega/8S\nu_f)$; S is the stiffness obtained from Eshelby's theory, and Ω is the atomic volume. Eq. (3) signifies that the free volume creation rate is proportional to the applied stress (σ) and the evolved strain rate ($\frac{d\varepsilon}{dt}$) during rolling. Therefore, the free volume is created continuously due to the application of stress, and the same is annihilated by the structural relaxation during the atomic rearrangements upon further rolling. The enhanced compressive strength of the CR specimens is due to the dominance of higher relaxation rate than that of free volume creation rate leading to the densification of the glassy phase [50]. Such deformation induced relaxation and densification of the glassy structure must be linked with the observed improvement of the strength and plasticity, which has also been reported earlier [44,50–53]. The presence of structurally relaxed glassy phase in the CR specimens has also been confirmed by the step scan MTDSC studies.

5. Conclusions

The following conclusions have been derived from the above investigation:

- The precise thermo-analytical measurements using step-scan MTDSC revealed a decrease of T_g by 16.9 K and increase of ΔT_x by 14.4 K upon cold rolling of $Zr_{55}Cu_{30}Ni_5Al_{10}$ ribbons and plates.
- The decrease of the T_g in the CR specimens reduces the STZ activation energy due to the evolution of a dense and relaxed glassy phase. At higher stress level, the large size STZs will form, and further densification occurs. The free volume is continuously being annihilated upon structural relaxation during rolling towards the formation of more stable glassy structure.
- Even though nano-voids have been formed locally in the SBs but the over all free volume in the structure has decreased. Furthermore, the rolling homogenizes the free volume distribution throughout the glassy phase, and reduces the quenched-in stresses in the as-cast specimens. As a result, both the compressive yield strength and plasticity have increased upon rolling.

Acknowledgments

The authors acknowledge the technical assistance of S. Maity and R. Kundu, and financial supports by Sponsored Research and Industrial Consultancy, IIT Kharagpur through SGBSI and SGIRG projects.

Appendix A. Supplementary data

Supplementary data to this article can be found online at https://doi.org/10.1016/j.msea.2019.138102.

References

[1] C.A. Angell, The glass transition, Curr. Opin. Solid State Mater. Sci. 1 (1996) 578–585.
[2] C.A. Angell, Perspective on the glass transition, J. Phys. Chem. Solids 46 (1988) 863–871.
[3] A. Inoue, Stabilization of metallic supercooled liquid and bulk amorphous alloys, Acta Mater. 48 (2000) 279–306.
[4] C. Suryanarayana, A. Inoue, Bulk Metallic Glasses, second ed., CRC Press, Taylor & Francis Group, Florida, 2017.
[5] W.L. Johnson, K. Samwer, A universal criterion for plastic yielding of metallic glasses with a $(T/T_g)^{2/3}$ temperature dependence, Phys. Rev. Lett. 95 (2005) 195501–195505.
[6] P.G. Debenedetti, F.H. Stillinger, Supercooled liquids and the glass transition, Nature 410 (2001) 259–267.
[7] W. Guo, R. Yamada, J. Saida, Rejuvenation and plasticization of metallic glass by deep cryogenic cycling treatment, Intermetallics 93 (2018) 141–147.
[8] J. Saida, R. Yamada, M. Wakeda, S. Ogata, Thermal rejuvenation in metallic glasses, Sci. Technol. Adv. Mater. 18 (2017) 152–162.
[9] Y. Tong, W. Dmowski, H. Bei, Y. Yokoyama, T. Egami, Mechanical rejuvenation in bulk metallic glass induced by thermo-mechanical creep, Acta Mater. 148 (2018) 384–390.
[10] A.L. Greer, Y.H. Sun, Stored energy in metallic glasses due to strains within the elastic limit, Philos. Mag. A 96 (2016) 1643–1663.
[11] P. Ross, S. Küchemann, P.M. Derlet, H.B. Yu, W. Arnold, P. Liaw, K. Samwer, R. Maass, Linking the macroscopic rejuvenation to nano-elastic fluctuations in a metallic glass, Acta Mater. 138 (2017) 111–118.
[12] H.B. Yu, W.H. Wang, K. Samwer, The β relaxation in metallic glasses: an overview, Mater. Today 16 (2013) 183–191.
[13] M. Wakeda, J. Saida, J. Li, S. Ogata, Controlled rejuvenation of amorphous metals with thermal processing, Sci. Rep. 5 (2015) 10545–10553.

[14] G. Riontino, M. Baricco, Structural relaxation in metallic glasses, Philos. Mag. A B 56 (1987) 177–183.
[15] G. Kumar, D. Rector, R.D. Conner, J. Schroers, Embrittlement of Zr-based bulk metallic glasses, Acta Mater. 57 (2009) 3572–3583.
[16] P. Murali, U. Ramamurty, Embrittlement of as bulk metallic glass due to sub-T_g annealing, Acta Mater. 53 (2005) 1467–1478.
[17] T.W. Wu, F. Spaepen, The relation between embrittlement and structural relaxation of an amorphous metal, Philos. Mag. A B 61 (1990) 739–750.
[18] A.S. Argon, H.Y. Kuo, Plastic flow in a disordered bubble raft (an analog of a metallic glass), Mater. Sci. Eng. A 39 (1979) 101–109.
[19] A.S. Argon, Plastic deformation in metallic glasses, Acta Metall. 27 (1978) 47–58.
[20] M. Stolpe, J.J. Kruzic, R. Busch, Evolution of shear bands, free volume and hardness during cold rolling of a Zr-based bulk metallic glass, Acta Mater. 64 (2014) 231–240.
[21] J. Das, M.B. Tang, K.B. Kim, R. Theissmann, F. Baier, W.H. Wang, J. Eckert, "Work-hardenable" ductile bulk metallic glass, Phys. Rev. Lett. 94 (2005) 205501–205505.
[22] J. Pan, K.C. Chan, Q. Chen, L. Liu, Enhanced plasticity by introducing icosahedral medium-range order in ZrCuNiAl metallic glass, Intermetallics 24 (2012) 79–83.
[23] M.H. Lee, K.S. Lee, J. Das, J. Thomas, U. Kühn, J. Eckert, Improved plasticity of bulk metallic glasses upon cold rolling, Scripta Mater. 62 (2010) 678–681.
[24] S. Xie, J.J. Kruzic, Cold rolling improves the fracture toughness of a Zr-based bulk metallic glass, J. Alloy. Comp. 694 (2017) 1109–1120.
[25] B. Shi, F. Wei, C. Li, J. Li, The introduction of highly dense shear bands and their effect on plastic deformation in Zr and Cu-based bulk metallic glasses, Mater. Sci. Eng. A 695 (2017) 265–269.
[26] Y. Xu, B. Shi, Z. Ma, J. Li, Evolution of shear bands, free volume, and structure in room temperature rolled $Pd_{40}Ni_{40}P_{20}$ bulk metallic glass, Mater. Sci. Eng. A 623 (2015) 145–152.
[27] Y. Xu, B. Shi, Effects of strain and strain rate on the evolution of shear bands for room temperature rolled $Pd_{40}Ni_{40}P_{20}$ bulk metallic glass, J. Non-Cryst. Solids 485 (2018) 74–81.
[28] Q. Zheng, D. Chen, L.K. Zhang, X.Y. Zhao, A.L. Zhang, Effect of ceramic rolling on the mechanical properties of $Zr_{54}Cu_{38}Al_8$ bulk metallic glass, Mater. Sci. Eng. A 592 (2014) 64–69.
[29] S. Scudino, K.B. Surreddi, Shear band morphology and fracture behavior of cold-rolled $Zr_{52.5}Ti_5Cu_{18}Ni_{14.5}Al_{10}$ bulk metallic glass under tensile loading, J. Alloy. Comp. 708 (2017) 722–727.
[30] M. Hu, Y. Hu, Effect of cold rolling on thermal stability of $Zr_{55}Al_{10}Ni_5Cu_{30}$ bulk metallic glass, Adv. Mater. Res. 490 (2011) 239–242.
[31] Y. Zhang, W.H. Wang, A.L. Greer, Making metallic glasses plastic by control of residual stress, Nat. Mater. 5 (2006) 857–860.
[32] M.H. Lee, J. Das, K.S. Lee, U. Kühn, J. Eckert, Effect of prestraining on the deformation and fracture behavior of $Zr_{44}Ti_{11}Cu_{9.8}Ni_{10.2}Be_{25}$, Intermetallics 18 (2010) 1902–1907.
[33] Q.P. Cao, J.F. Li, Y.H. Zhou, A. Horsewell, J.Z. Jiang, Effect of rolling deformation on the microstructure of bulk $Cu_{60}Zr_{20}Ti_{20}$ metallic glass and its crystallization, Acta Mater. 54 (2006) 4373–4383.
[34] Q.P. Cao, J.W. Liu, K.J. Yang, F. Xu, Z.Q. Yao, A. Minkow, H.J. Fecht, J. Ivanisenko, L.Y. Chen, X.D. Wang, S.X. Qu, J.Z. Jiang, Effect of pre-existing shear bands on the tensile mechanical properties of a bulk metallic glass, Acta Mater. 58 (2010) 1276–1292.
[35] Y. Yokoyama, K. Yamano, K. Fukaura, H. Sunada, A. Inoue, Enhancement of ductility and plasticity of $Zr_{55}Cu_{30}Al_{10}Ni_5$ bulk glassy alloy by cold rolling, Mater. Trans., JIM 42 (2001) 623–632.
[36] P.P. Jana, J. Das, Precise estimation of glass transition and crystallization temperatures of $Zr_{55}Cu_{30}Ni_5Al_{10}$ metallic glass using step-scan modulated temperature differential scanning calorimeter, Thermochim. Acta 660 (2018) 18–22.
[37] K.K. Song, S. Pauly, Y. Zhang, S. Scudino, P. Gargarella, K.B. Surreddi, U. Kühn, J. Eckert, Significant tensile ductility induced by cold rolling in $Cu_{47.5}Zr_{47.5}Al_5$ bulk metallic glass, Intermetallics 19 (2011) 1394–1398.
[38] J. Kobata, T. Kimura, Y. Takigawa, T. Uesugi, H. Kimura, K. Higashi, Effect of pre-introduced shear bands direction on deformation behavior in $Zr_{55}Al_{10}Ni_5Cu_{30}$ bulk metallic glass, Mater. Trans., JIM 50 (2009) 2355–2358.
[39] J.M. Park, K.R. Lim, E.S. Park, S. Hong, K.H. Park, J. Eckert, D.H. Kim, Internal structural evolution and enhanced tensile plasticity of Ti-based bulk metallic glass and composite via cold rolling, J. Alloy. Comp. 615 (2014) S113–S117.
[40] J. Li, Z.L. Wang, T.C. Hufnagel, Characterization of nanometer-scale defects in metallic glasses by quantitative high-resolution transmission electron microscopy, Phys. Rev. B 65 (2002) 144201–144207.
[41] B. Vishwanadh, S.K. Sharma, P.K. Pujari, R. Kishore, G.K. Dey, R. Tewari, Influence of free volume and medium-range order on the deformation response of rapidly solidified and bulk Zr-based ($Zr_{52}Ti_6Al_{10}Cu_{18}Ni_{14}$) metallic glass, Philos. Mag. A 93 (2013) 3442–3471.
[42] Z.P. Lu, C.T. Liu, Y. Li, Glass transition and crystallization of Mg–Ni–Nd metallic glasses studied by temperature-modulated DSC, Intermetallics 12 (2004) 869–874.
[43] Z.P. Lu, Y. Li, S.C. Ng, Y.P. Feng, Study of glass transition of metallic glasses by temperature-modulated differential scanning calorimetry (MDSC), Thermochim. Acta 65 (2000) 357–358.
[44] A. Slipenyuk, J. Eckert, Correlation between enthalpy change and free volume reduction during structural relaxation of $Zr_{55}Cu_{30}Al_{10}Ni_5$ metallic glass, Scripta Mater. 50 (2004) 39–44.
[45] L. Battezzati, G. Riontino, M. Baricco, A. Lucci, F. Marino, A DSC study of the structural relaxation in metallic glasses prepared with different quenching rates, J. Non-Cryst. Solids 61 & 62 (1984) 877–882.
[46] C.A. Schuh, T.C. Hufnagel, U. Ramamurty, Mechanical behavior of amorphous alloys, Acta Mater. 55 (2007) 4067–4109.
[47] M.L. Falk, J.S. Langer, Dynamics of viscoplastic deformation in amorphous solids, Phys. Rev. E 57 (1998) 7192–7205.
[48] Y. Hu, J.F. Li, P.N. Zhang, Y.H. Zhou, Effect of cold rolling on glass transition of $Zr_{55}Al_{10}Ni_5Cu_{30}$ bulk metallic glass, Trans. Nonferrous Metals Soc. China 20 (2010) 78–81.
[49] M. Heggen, F. Spaepen, M. Feuerbacher, Creation and annihilation of free volume during homogeneous flow of a metallic glass, J. Appl. Phys. 97 (2005) 033506–033514.
[50] Z.T. Wang, J. Pan, Y. Li, C.A. Schuh, Densification and strain hardening of a metallic glass under tension at room temperature, Phys. Rev. Lett. 111 (2013) 135504–135509.
[51] F. Meng, K. Tsuchiya, Seiichiro II, and Y. Yokoyama, Reversible transition of deformation mode by structural rejuvenation and relaxation in bulk metallic glass, Appl, Phys. Lett. 101 (2012) 121914.
[52] S.V. Ketov, Y.H. Sun, S. Nachum, Z. Lu, A. Checchi, A.R. Beraldin, H.Y. Bai, W.H. Wang, D.V. Louzguine-Luzgin, M.A. Carpenter, A.L. Greer, Rejuvenation of metallic glasses by non-affine thermal strain, Nature 524 (2015) 200–203.
[53] J. Pan, Y.X. Wang, Q. Guo, D. Zhang, A.L. Greer, Y. Li, Extreme rejuvenation and softening in a bulk metallic glass, Nat. Commun. 9 (2018) 560–569.